Polymer models reveal how chromatin modification can modulate force at the kinetochore

Josh Lawrimore, Solenn C. de Larminat, Diana Cook, Brandon Friedman, Ayush Doshi, Elaine Yeh, and Kerry Bloom*
Biology Department, The University of North Carolina at Chapel Hill, Chapel Hill, NC 27599

ABSTRACT **A key feature of chromosome segregation is the ability to sense tension between sister kinetochores. DNA between sister kinetochores must be packaged in a way that sustains tension propagation from one kinetochore to its sister, approximately 1 micron away. A molecular bottlebrush consisting of a primary axis populated with a crowded array of side chains provides a means to build tension over length scales considerably larger than the stiffness of the individual elements, that is, DNA polymer. Evidence for the bottlebrush organization of chromatin between sister kinetochores comes from genetic, cell biological, and polymer modeling of the budding yeast centromere. In this study, we have used polymer dynamic simulations of the bottlebrush to recapitulate experimental observations of kinetochore structure. Several aspects of the spatial distribution of kinetochore proteins and their response to perturbation lack a mechanistic understanding. Changes in physical parameters of bottlebrush, DNA stiffness, and DNA loops directly impact the architecture of the inner kinetochore. This study reveals that the bottlebrush is an active participant in building tension between sister kinetochores and proposes a mechanism for chromatin feedback to the kinetochore.**

Monitoring Editor
Dennis Discher
University of Pennsylvania

Received: Feb 11, 2022
Revised: May 10, 2022
Accepted: Jun 6, 2022

INTRODUCTION

The centromere appears as the primary constriction in a condensed mitotic chromosome. The surface of the centromere provides the binding site for the kinetochore, while its interior domain is the site of mechanical linkage between sister kinetochores. Correct bipolar attachment of sister chromatids to the mitotic spindle leads to microtubule-based tension between sister kinetochores. Through chromosome manipulation with calibrated microneedles, Nicklas and colleagues established that tension at the kinetochore is the primary source of information to ensure error-free chromosome segregation (Nicklas and Koch, 1969; Henderson and Koch, 1970; Li and Nicklas, 1995).

The mechanism of mechanical linkage between sister centromeres has been attributed to cohesin, a ring-like protein complex required for sister chromatid cohesion. In budding yeast, cohesin is concentrated in a 30–50-kb region surrounding the point centromeres, known as the pericentromere, bounded by sites of divergent gene transcription (Paldi *et al.*, 2020). However, cohesin does not reside between sister kinetochores when visualized in live cells. Cohesin appears as a cylinder surrounding the central spindle between sister kinetochores (Figure 1B). Alternative models that do not invoke cohesin as the primary means of mechanical linkage within the centromere are required to reconcile the radial displacement of cohesin relative to sister kinetochores.

Modeling the yeast pericentromere as a molecular bottlebrush makes predictions that quantitatively match numerous experimental observations. These include the 1) radial displacement and cylindrical appearance of cohesin in metaphase, 2) the spatial segregation of condensin and cohesin, 3) the fraction of off- (90%) and on- (10%) spindle axis pericentric DNA, 4) the dynamics of pericentric DNA spots labeled with the lacO system, and 5) the correlated motion of DNA spots at different centromeres (Lawrimore *et al.*, 2016, 2018).

This article was published online ahead of print in MBoC in Press (http://www.molbiolcell.org/cgi/doi/10.1091/mbc.E22-02-0041) on June 15, 2022.

*Address correspondence to: Kerry Bloom (kerry_bloom@unc.edu).

Abbreviations used: b, Kuhn length; C-loop, centromere loop; ChIP, chromatin Immunoprecipitation; FWHM, full-width-half-max; GFP, green fluorescent protein; k_BT, Boltzmann's constant; k_s, spring constant; L_p, persistence length; LacO, lac operator; LacI, lac repressor; PCR, polymerase chain reaction; R_g, radius of gyration.

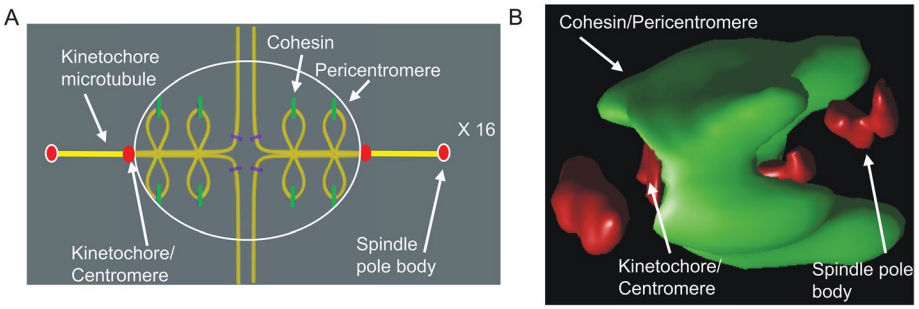

FIGURE 1: Simulated vs. experimental images of the pericentromeric region in metaphase in budding yeast. (A) Schematic of the position of the kinetochore and centromere (red oval) and pericentromere (DNA loops in yellow, cohesin in green, within large gray oval) of an individual sister chromatid pair in metaphase (spindle pole [red/white ovals] and kinetochore microtubules [yellow bar]). The schematic is derived from studies of the position of lacO arrays integrated proximal to the centromere and the displacement of cohesin from the main spindle microtubule axis. (B) Deconvolved image of the pericentromere from a live cell containing cohesin, kinetochore, and spindle pole body proteins fused to fluorescent proteins (cohesin, Smc3-GFP; kinetochore, Ndc80-mCherry; spindle pole, Spc29-RFP). In budding yeast, the 32 centromeres (16 sister chromatid pairs) are clustered on the mitotic spindle in metaphase. The image depicts barrel-shaped structure of cohesin (green) and pericentromere chromatin as they appear in a live cell relative to separated sister kinetochores (inner red foci) and the spindle pole bodies (outer red foci). Note that cohesin and the pericentromere surround the central microtubule spindle (extending between the two spindle pole bodies) and extend laterally beyond the centromere and kinetochore microtubules. The schematic is drawn to scale, with the entire length of the spindle ~1.5 microns.

A molecular bottlebrush consists of a primary axis or loop, with numerous side chains, or secondary loops (Figure 1A). This configuration amplifies tension along the primary axis due to molecular crowding of the side chains, providing a means to stiffen the centromere over a micron length scale. In budding yeast, the point centromeres lie at the apex of the primary axis, where they interact with kinetochores. The pericentromere subloops are the 30–50-kb region flanking the point centromere surrounding the primary axis. Condensin lies along the spindle axis, where it extrudes DNA loops that form the basis of the bottlebrush (Stephens *et al.*, 2013a,b). Cohesin acts as molecular slip links that diffuse to the thermodynamically favored position in the loop. Cohesin functions to compact the loops, contributing to the mechanism of tension amplification along the primary axis between sister kinetochores. The model quantitatively predicts the radial displacement of cohesin from the sister kinetochore axis and its appearance as a barrel surrounding the central spindle (Figure 1B) (Yeh *et al.*, 2008) and provides the physical basis for how pulling forces from the mitotic spindle are transmitted through the centromere region between sister kinetochores.

The centromeres are attached to kinetochore microtubules via the kinetochore (reviewed in Biggins, 2013; Dhatchinamoorthy *et al.*, 2017). Each kinetochore is a cylindrical structure 70 nm in length and ~35 nm in diameter that encircles the plus end of microtubule at one end (outer kinetochore) and is purported to taper to the centromere-specific histone H3 variant, Cse4 (inner kinetochore) at the surface of the centromere. Individual kinetochores from the 16 chromosomes are clustered in a ring-like structure due to the cylindrical arrangement of kinetochore microtubules around the central spindle (Winey *et al.*, 1995; O'Toole *et al.*, 1999) (Figure 2A). Fluorescently labeled inner kinetochore proteins (Ame1, Cse4, centromere proximal) appear wider in a direction perpendicular to the spindle axis than the outer kinetochore proteins (Haase *et al.*, 2013). The outer kinetochore proteins (microtubule proximal, i.e., Ndc80) appear more compact than the inner proteins. Using artificial intelligence–assisted forward modeling of simulated images, we were able to determine the magnitude of radial displacement of the inner kinetochore proteins observed in vivo. Inner kinetochore complexes are displaced 25–50 nm from the spindle axis relative to the outer components (Figure 2). The mechanism by which the inner centromere–proximal kinetochore complexes are offset from the outer microtubule–proximal kinetochore is not evident from the arrangement or dynamics of kinetochore microtubules.

The proximal relationship between pericentromeric loops and the inner kinetochore is indicative of biochemical or mechanical communication between these two macromolecular complexes. Experimental evidence for mechanical linkage was obtained through observations of cohesin and the inner kinetochore following mild perturbation of the mitotic spindle (Haase *et al.*, 2012). At low concentrations of benomyl the spindle checkpoint machinery prevents the accumulation of errors in chromosome segregation and is permissive for cell growth (Pearson *et al.*, 2003). Under these conditions, the cohesin barrel and pericentric DNA loops expand to occupy a greater area, while chromatin-proximal kinetochore components exhibit the inverse trend (Haase *et al.*, 2012). The inner kinetochore components Ame1 and Cse4 decrease in their width in a direction perpendicular to the spindle axis (Haase *et al.*, 2012). The cohesin expansion/inner kinetochore contraction are dependent on histone H2A phosphorylation by the Bub1 kinase.

Chromatin modification, including histone phosphorylation, is known to influence the mechanical properties of chromatin, providing a means to account for the observed expansion/contraction (Brower-Toland *et al.*, 2005; Basu *et al.*, 2021). The flexibility of the chromatin fiber is defined by a parameter known as the persistence length (L_p). L_p is the length scale over which the chain is stiff, mathematically when the tangent vectors along the monomer become uncorrelated. Changes in L_p have a direct effect on the chromatin spring constant ($k_s = K_B T/L_p^2$). Increasing L_p reduces the spring constant and increases the area the chain occupies ($R_g R^2 = NL_p^2$, where R_g = radius of gyration and N = number of L_p monomers), while decreasing L_p increases the spring constant, decreasing the area occupied. The ability to tune the chromatin spring via histone modifications contributes to maintaining centromere tension throughout cycles of microtubule growth and shortening and chromosome oscillation.

To test whether changes in persistence length are a feasible means to account for the magnitude and direction of inner kinetochore contraction following spindle perturbation, we employed a polymer model of the budding yeast pericentromere (Lawrimore *et al.*, 2016). The model is based on the geometry of pericentromere DNA loops and their thermodynamically favored states. In this study, we determined whether increasing the stiffness of pericentric chromatin in the simulation would result in lower tension at the centromere, alter the three-dimensional direction of the force at the centromere, reduce chromatin motion of the loops, and expand the cohesin barrel distribution. We find that increasing the persistence length of pericentric chromatin is sufficient to recapitulate each of

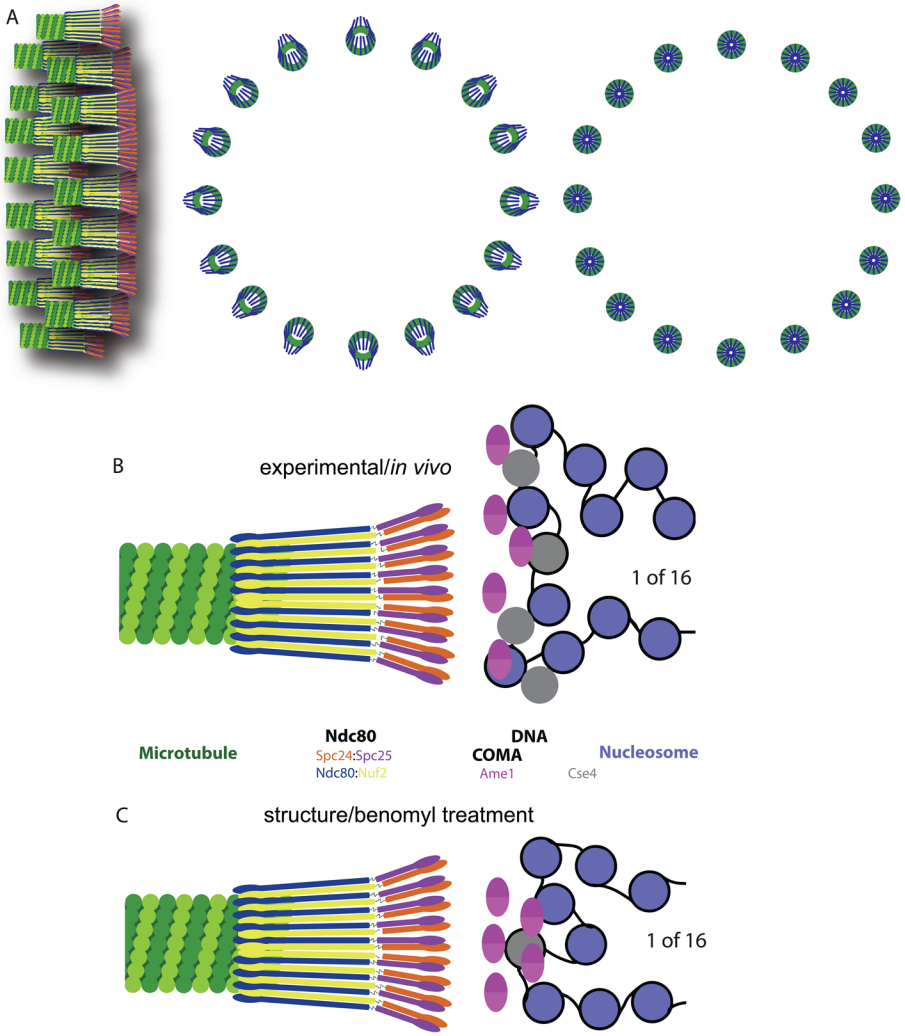

FIGURE 2: Schematic of ensemble of 16 budding yeast kinetochores (top) and individual kinetochores (bottom). (A) The 16 kinetochores in the half spindle are clustered as a consequence of the cylindrical arrangement of 16 kinetochore microtubules in metaphase (left). The diameter of the cluster of 16 kinetochores is ~250 nm. End-on views (spindle perpendicular to the page of view) illustrate the angular displacement of the inner kinetochore (Ame1) (middle) and the contraction of the inner kinetochore following gentle spindle perturbation through benomyl treatment (right). (B) An individual kinetochore is 70 nm in length from the Ndc80 microtubule binding module (colored rods surrounding microtubule plus end, left) to the centromere-specific histone variant Cse4 (gray circles, right). Ndc80 is indicated as uniformly distributed; however, not all molecules may be bound to microtubules (Yoo *et al.*, 2018). There are excess Cse4 molecules than can be accounted for by the single Cse4 nucleosome incorporated at the 117-base-pair centromere DNA (Haase *et al.*, 2013). (C) Upon benomyl treatment, the inner kinetochore contracts in size, as indicated by the reduced area occupied by the COMA complex (Ame1 in purple) (Haase *et al.*, 2012, 2013).

the aforementioned observations, thus providing a simple mechanism for lowering kinetochore tension upon disruption of mitotic spindle integrity and resolving the paradox of the expansion of the pericentric chromatin but contraction of the inner kinetochore distribution.

RESULTS

Spindle perturbation disproportionally affects the inner versus outer kinetochore

We implemented an automated analysis software pipeline, CellStarSelect, in order to acquire, segment, and normalize images with no direct human measurement. To validate the method, we asked whether the results recapitulate three prior observations that 1) the spindle length, as measured by the distance between the two spindle pole foci (Spc42-mCherry) decreases (Figure 3, A and B), 2) the spot width of inner kinetochore protein Ame1 foci (Ame1-GFP), as measured by the full-width half maximum value of a Gaussian distribution drawn perpendicular to the spindle axis, decreases (Figure 3C), and 3) the spot width of the spindle pole foci (Spc42-mCherry) is not altered by benomyl treatment (Figure 3D). The CellStarSelect results confirm and extend the observations made in Haase *et al.* (2012). The schematic in Figure 2 illustrates the behavior of the ensemble of 16 kinetochores (observed in the microscope) relative to an individual kinetochore, which cannot be distinguished from one another in metaphase due to their proximity (about 60 nm between kinetochores) and the diffraction limit of the light microscope. The contraction of the inner kinetochore is not accompanied by a geometrical change of the outer kinetochore (Haase *et al.*, 2012). These findings are indicative of forces that impinge specifically on the inner kinetochore.

The dominant feature of the bottlebrush is the crowding of side chains that lead to "stiffening" of the primary axis, providing a mechanism to build tension despite the inherent floppiness of DNA/chromatin. The side chains also exert a repulsive radial force. The radial force is the tendency of the chains to expand beyond their degree of confinement around the spindle axis. The most thermodynamically stable configuration of DNA is a random walk with a radius of gyration defined as $R_g^2 = nb^2$ (n = number of segments and b = Kuhn length, or 2× L_p). There is approximately 800 kb of DNA in the bottlebrush. The radius of gyration for 800 kb of DNA is about 5 microns, or about 5× the radius of the budding yeast nucleus. The radial force is the tendency for the pericentric DNA loops to expand to the 5 micron radius of gyration and is predicted to impinge on the structure of the inner kinetochore.

The inner kinetochore Ame1-GFP foci were analyzed for changes in total signal intensity and compaction (Figure 4). There was no significant difference in the total signal integrated intensities (after background subtraction; see *Materials and Methods*) of the Ame1-GFP signal upon benomyl treatment (Figure 4A). The total signal mean intensity (intensity per pixel) was significantly increased in cells treated with 313 μM benomyl (Figure 4B). There was no significant difference in the total mean intensity per volume (Figure 4C); however, the maximum intensity of a given kinetochore spot was found to be significantly larger in cells treated with 313 μM benomyl (Figure 4D). Thus, when cells were treated with 313 μM benomyl, a

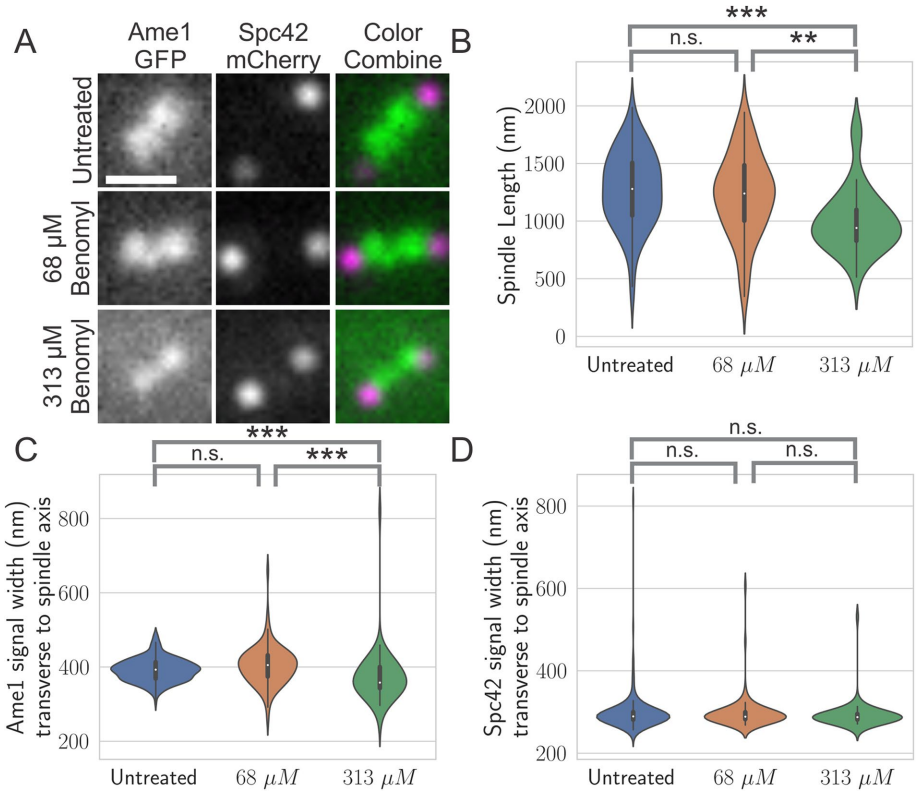

FIGURE 3: Automatic foci analysis confirms that Ame1-GFP foci contract perpendicular to the spindle axis. (A) Representative images of Ame1-GFP (green) and Spc42-mCherry (magenta). (B) Violin plot of spindle length. (C) Violin plot of Ame1-GFP spot width (perpendicular to the spindle axis). (D) Violin plot of Spc42-mCherry spot width. The n.s. indicates P value > 0.05, the ** indicates P value < 0.05, the *** indicates P value < 0.001 by Kruskal–Wallis test. For Untreated, n = 105; benomyl 68 μM, n = 49; benomyl 313 μM, n = 30. Scale bar = 1 micron.

subset of the total Ame1-GFP signal became more compact, resulting in a larger voxel intensity within the kinetochore foci. These observations are consistent with compaction of the inner kinetochore distribution, rather than a loss of inner kinetochore protein signal.

Reduction in spot width of the inner kinetochore can be reproduced by reducing the radial displacement of inner kinetochores

We utilized a three-dimensional kinetochore simulator representing the kinetochore as a 70 nm linear rod to distinguish mechanisms of kinetochore responsiveness to microtubule perturbations (Lawrimore *et al.*, 2019). The interface of the StaticKinet MATLAB application was used to generate simulated fluorescent images of kinetochore models. This application allows users to generate custom three-dimensional models of the budding yeast mitotic spindle and kinetochore complex. The angle of the rod relative to the kinetochore microtubule to which it is bound can be increased to cause the inner kinetochore protein to become radially displaced (Lawrimore *et al.*, 2019). We created 100 simulated z-stacks of radially displaced kinetochore from 0 to 90° (Figure 5A). As expected, the radial displacement of the kinetochore did not alter the spot width of the simulated N-terminus of Nuf2, as that end of the kinetochore remained bound to the kinetochore microtubule (Figure 5B). In contrast, the spot width of the simulated Ame1 foci increased with larger displacement angles (Figure 5C). We compared the experimental mean spot widths of Ame1-GFP from untreated and 313 μM benomyl–treated strains and found that a decrease of 10° (from 30 to 20°) corresponded to the decrease in spot width observed experimentally (Figures 3C and 5C). Thus, a reduction in radial pulling force away from the spindle axis is sufficient to recapitulate a reduction in the experimentally measured inner kinetochore spot width.

Increasing subloop size and increasing chromatin stiffness both reduce force on centromere masses in polymer simulations

To determine whether alteration of subloop size and/or chromatin stiffness of the pericentric chromatin loops might impact the pulling force on the centromeres, we analyzed the motion of centromere masses in simulations of the pericentromere with different subloop sizes and chromatin bending stiffnesses. The centromere masses are the beads at the apex of the primary loop, proximal to the microtubule plus ends (shown individually in Figure 1A, and ensemble of 16 as observed in the microscope in Figure 6A). Pericentromere loops have been estimated to range from two to four loops in vivo (live cell modeling [Stephens *et al.*, 2013a]) to a single loop ~20 kb (ChIP [Paldi *et al.*, 2020]) per chromosome. We have used ChromoShake, a three-dimensional simulator designed to find the thermodynamically favored states for given chromosome geometries to estimate the number and size of the loops (Lawrimore *et al.*, 2016). Using model convolution to attain subpixel accuracy, we have shown that cohesin and condensin are sensitive readouts of the number and displacement of chromatin loops (Stephens *et al.*, 2013b). Two to four 10-kb DNA loops per sister chromatid predict the experimental observations of condensin and cohesin (Lawrimore *et al.*, 2016). Chromatin bending stiffness was measured as the persistence length (L_p; see *Materials and Methods*). L_p reflects the length scale over which tangent vectors at the ends of a monomer segment of the polymer remain correlated and is linearly related to bending stiffness (Rubinstein and Colby, 2003). The persistence length of naked DNA is 50 nm (Hagerman, 1988). We determined the force on the centromeres in simulations by measuring the displacement of the masses composing the centromeres from their initial positions. Each centromere is composed of two monomers, each of which experiences 100,000-fold more drag force than a typical monomer unit in the body of the bottlebrush. The increased drag force on the centromere masses is a surrogate for microtubule attachment in vivo and effectively pins the pericentromere simulations in space. The centromere masses are gradually pulled inward as the simulation equilibrates. Increasing the size of the subloops and increasing the persistence length of chromatin both resulted in a drop in the force on centromere masses (Figure 6, B and C). The drop in the force on centromeres in simulations with 10-kb or larger loops was anticipated due to the bottlebrush force, generated by the steric repulsion of the subloops, causing an extensional force on the chromatin (Panyukov *et al.*, 2009a,b; Lawrimore *et al.*, 2016). The high variance in simulations with 6-kb loops

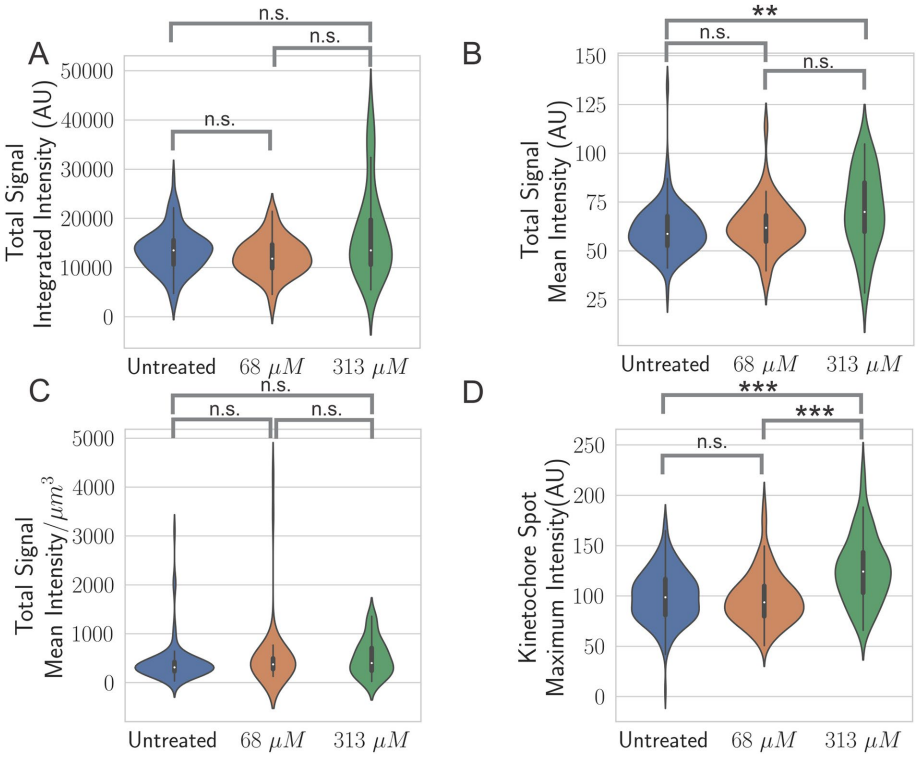

FIGURE 4: Benomyl treatment compacts the Ame1-GFP kinetochore foci. Violin plots of the total signal integrated intensity (A), the total signal mean intensity (B), the total signal mean intensity per cubic micron (C), and the kinetochore spot maximum intensity (D). The n.s. indicates P value > 0.05, the ** indicates P value < 0.01, the *** indicates P value < 0.001 by Kruskal–Wallis test. For Untreated, $n = 105$; benomyl 68 μM, $n = 49$; benomyl 313 μM, $n = 30$.

reflects a mechanism by which the network buffers variation intrinsic to any single loop. As the size of loops decreases (less than 10 kb) there is an increased chance that these loops will be devoid of cohesin. When the loops are 10 kb or greater, there is an increasing chance that they contain cohesin and therefore impact one another, acting as shock absorbers for the chromatin. This constant impact acts as a buffering force as variance in individual loops will be resisted by the neighboring loops.

The drop in force on centromeres in simulations with increasing persistence lengths is due to the chromatin becoming a weaker entropic spring (Smith *et al.*, 1996). As the persistence length increases, there are fewer entropic states for the polymer to adopt, leading to a weaker entropic spring ($k_s = k_BT/L_p^2$). Both increasing the subloop size and increasing the persistence length resulted in a reduction in the tension in the springs attached to the centromere masses (Figure 6, D and E) and a reduction in the tension in the springs of chromatin within the main centromere loop (C-loop, all chromatin not in the subloops) of each sister chromatid (Figure 6, F and G). These findings are indicative of the molecular crowding provided by the packing of pericentromere DNA between the sister kinetochores and the critical role for DNA loops in how tension is propagated over the approximately 800–1000 nm between sister kinetochores. Any model of the pericentromere must be accountable for this density of loops.

Increasing chromatin stiffness, but not subloop size, reduces radial force on centromeres

The treatment of budding yeast with low doses of benomyl results in both the reduction of tension within kinetochores (Suzuki *et al.*, 2016) and the decrease of the distributions of inner kinetochore proteins perpendicular to the spindle axis (Figure 2 and [Haase *et al.*, 2012]). To determine whether altering the subloop size or the chromatin stiffness would result in a reduction in the axial (parallel to the spindle axis) and/or radial force (perpendicular to the spindle axis), we measured the force on centromere masses in the axial and radial directions (Figure 7A). The axial force on centromere masses was reduced by increasing both subloop size and chromatin stiffness (Figure 7, B and C). Increasing loop size reduces axial force due to reduced crowding of the chains (longer chains occupy a greater volume). The disproportionate effect on the axial versus radial force reflects this topological arrangement. Expansion of the chains into a larger volume tends to reduce the length of the primary axis of the brush. Chain fluctuations orthogonal to the primary axis occur (radial force) but are dominated by overall shortening of the primary axis. The radial force on centromeres was not significantly changed by increasing loop size (Figure 7D) but was reduced by increasing chromatin stiffness (Figure 7E). Moreover, the pulling force on the kinetochore is reduced upon low-dose benomyl treatment (Suzuki *et al.*, 2016). While increasing loop size had a modest effect on the force, the stiffness of the polymer has a much greater effect on the radial force applied to centromeres.

Increasing chromatin stiffness recapitulates the reduction of chromatin motion and expansion of pericentric cohesin distribution

Increasing chromatin stiffness in ChromoShake simulations of the pericentromere was sufficient to reduce the total and radial forces on centromere masses, recapitulating the observations in Suzuki *et al.* (2016) and Haase *et al.* (2012). Previous studies have shown that yeast treated with low doses of benomyl also exhibit reduced chromatin motion (Haase *et al.*, 2012; Lawrimore *et al.*, 2015) and an expansion of the distribution of pericentric cohesion, referred to as the cohesin barrel, perpendicular to the spindle axis (Haase *et al.*, 2012). Previous work using ChromoShake simulations of pericentric chromatin had shown that increasing loop size increased the radial displacement of pericentric cohesin (Lawrimore *et al.*, 2016). To determine whether the small reduction in the motion of a 10-kb LacO/LacI-GFP array positioned 6.8 kb from CENXV upon benomyl treatment (Lawrimore *et al.*, 2015) could be recapitulated by increasing loop size, we labeled the same pericentric simulations with a simulated analogue of the 10-kb LacO/LacI-GFP array. Increasing the radial subloop size monotonically increased the motion of the simulated 10-kb array (Figure 8A). Thus, increasing loop size did not recapitulate the reduction in motion upon low-dose benomyl treatment.

We applied the same 10-kb array labeling scheme to the simulations of pericentric chromatin with 10-kb radial subloops with various simulated chromatin stiffness. We found that increasing

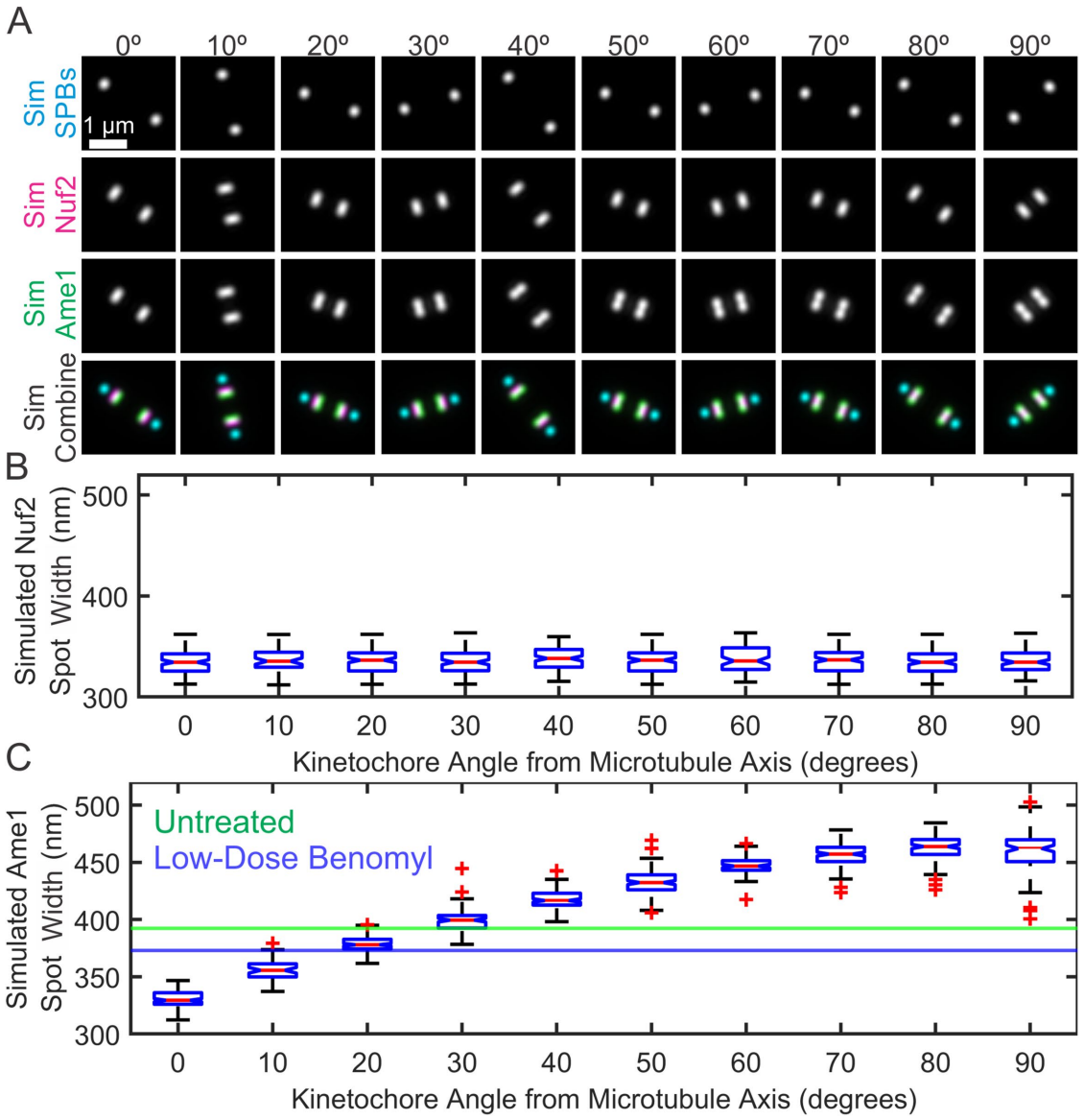

FIGURE 5: Decrease in radial displacement of kinetochore is sufficient to replicate reduction in Ame1 spot width in synthetic images. (A) Representative images of three-dimensional kinetochore and spindle pole body (SPB) simulations with different radial angles. Scale bar is 1 micron. Box plots of simulated Nuf2 (B) and Ame1 (C) spot widths vs. kinetochore angle from microtubule axis. Green and blue lines represent the mean spot width of untreated Ame1-GFP and 313 µM benomyl–treated Ame1-GFP, respectively (as determined in Figure 3).

simulated chromatin stiffness initially increased the motion of the 10-kb array, but the motion dropped in the simulation with the largest polymer stiffness (L_p = 500 nm) (Figure 8B). Thus, the relationship between the 10-kb array's motion and simulated chromatin stiffness is nonmonotonic. The nonmonotonicity between the mobility of subloops and chromatin stiffness is reminiscent of recent findings in He *et al.* (2020). Implementation of chromatin binding proteins and cross-linkers leads to a nonmonotonic relationship between mobility and chain stiffness in silico. In contrast, increasing the simulated chromatin stiffness monotonically increased the mean radial distance of the cohesin complexes in the simulation (Figure 8C). Thus, an increase in simulated chromatin stiffness can recapitulate the decrease in the 10-kb array's motion and the increase in the length of the cohesin distribution perpendicular to the spindle axis.

DISCUSSION

In silico chromatin modification of the pericentromere exerts force on the kinetochore

The kinetochore is a unique tension-sensitive coupling device that links stiff kinetochore microtubules to floppy chromatin at the surface of a condensed chromosome. How one structure integrates the divergent stiffness between these two substrates into a signal that accounts for the fidelity of chromosome segregation remains a mystery. Visual inspection of the kinetochore reveals its ability to physically respond to various environmental perturbations (Haase *et al.*, 2012). Activation of the spindle assembly checkpoint (via Bub1 kinase) stimulates the phosphorylation of histone (H2A) that manifests in a contraction of the inner kinetochore, independent of the outer kinetochore (Haase *et al.*, 2012). This is the first indication of structural plasticity within the yeast kinetochore.

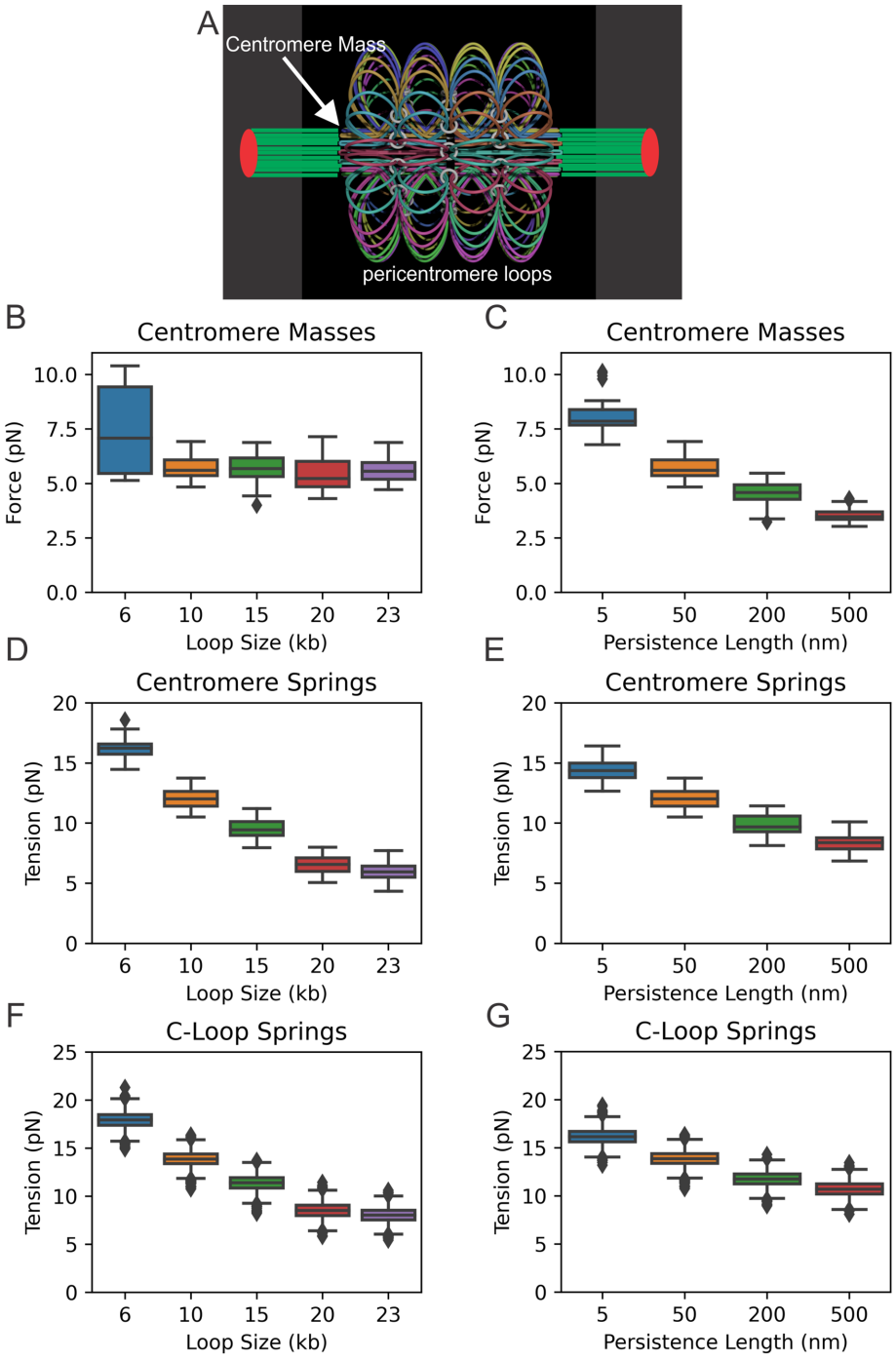

FIGURE 6: Increasing loop size and chromatin stiffness reduces pulling force on centromeres and tension on chromatin springs in simulations. (A) Starting configuration of pericentric chromatin in metaphase. The pericentric region 32 sister chromatids are clustered around the spindle axis in metaphase. The DNA is visualized as colored strands. Kinetochore microtubules (green rods) are nucleated from the spindle pole body (red disk). The 16 kinetochore microtubules in each half-spindle are cylindrically arrayed around interpolar microtubules extending about ¾ the length of the spindle (unpublished data). The centromere masses (indicated by white arrow) are the beads at the apex of the primary loop, representing the 117-base-pair centromere DNA sequence proximal to the kinetochore microtubule plus ends. Centromere springs are the springs connecting the centromere masses to the beads defining the pericentromere (pericentromere subloops). The C-loop springs are the springs along the primary axis (aligned with the kinetochore microtubules) or alternatively, all chromatin springs not in the orthogonal subloops. The sizes of the loops refer to the secondary loops orthogonal to the spindle axis. The number of pericentromeric subloops is constant in simulation. The length of the primary loop is determined from the distance between the cluster of sister kinetochores (~800 nm) and is invariant in simulation. The total length of the polymer in the model is ~800 kb DNA (25 kb/pericentromere × 2 sister strands × 16 chromosomes), dictated by the length of the primary axis and size of the subloops. Box plots comparing the force applied to centromere masses in simulations with various loop sizes but with a uniform persistence length of 50 nm (B) and various persistence lengths but with a uniform subloop size of 10 kb (C). Box plots comparing the tension on springs connected to centromere masses in simulations with various loop sizes (D) and persistence lengths (E). Box plots comparing the tension on the springs within the main centromere loops (C-loop; all chromatin springs not within subloops) in simulations with various loop sizes (F) and persistence lengths (G). Both DNA loop size and persistence length have a significant effect on the force on centromere mass, the tension on the springs connected to the centromere masses, and the tension on the C-loop springs (*P* value of Kruskal–Wallis test < 0.01 for all).

In this in silico study, we find that changing properties of chromatin stiffness in the pericentromere successfully recapitulates several in vivo observations of kinetochore behavior in response to microtubule perturbation. The contraction of the inner kinetochore is assessed as a reduction in the distribution of inner kinetochore COMA components. The contraction of the inner kinetochore can be quantitatively simulated by decreasing the radial displacement of the kinetochore (reducing the angle of deflection relative to the microtubule axis; Figure 5). Radial kinetochore displacement could be driven by outward-pushing forces from the compacted pericentromeric chromatin. The radial force exerted by the pericentric chromatin is reduced when the chromatin stiffness increases (chromatin persistence length L_p; Figure 7E). This counterintuitive result makes sense in light of the properties of an entropic spring, such as DNA/chromatin. The entropic spring force is inversely proportional to chromatin persistence length ($k_s \sim K_BT/L_p^2$; k_s = spring constant in N/nm, K_BT = Boltzmann constant [4.1 pN*nm], L_p = persistence length in nm). The longer the persistence length (and therefore the increased length scale over which chromatin is stiff), the fewer available states for the random coil to adopt. Less force is required to extend a chain that has fewer available states, and therefore the spring force decreases.

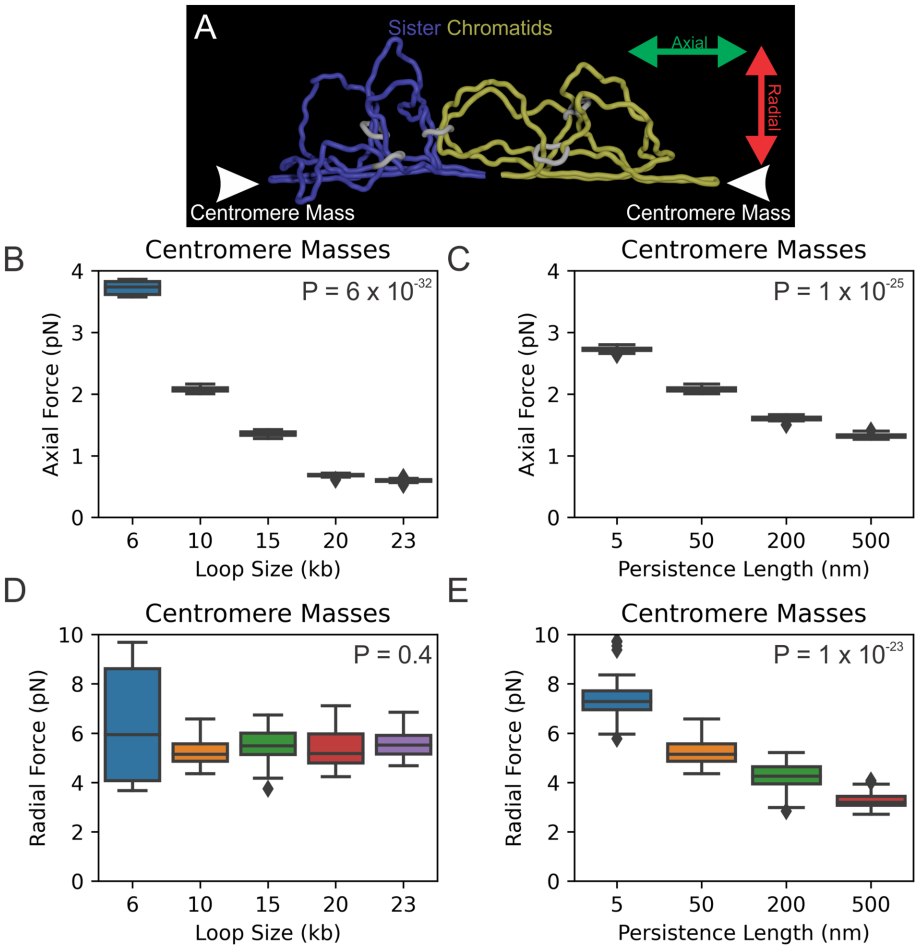

FIGURE 7: Increasing chromatin stiffness, not loop size, reduces radial force on centromere masses in simulation. (A) Visualization of one pair of sister chromatid strands after equilibration (15 million calculation time steps) highlighting the geometry of axial vs. radial force. White arrowheads indicate centromere masses at the apex of the primary loop. White rings are cohesin bound to sister chromatids. Axial dimension is parallel to the spindle axis and is the *Z*-dimension in the simulation. The radial dimension is orthogonal to the *Z*-dimension. Simulations in B–E are from the entire pericentromere composed of the 32 chromatids (Figure 6A). Box plots comparing the axial force in simulations with increasing subloop sizes (B) and increasing chromatin persistence length (C). Box plots comparing the radial force in simulations with increasing subloop sizes (D) and increasing chromatin persistence length (E). *P* values are from a Kruskal–Wallis test.

The persistence length of naked DNA reflects the chemical properties of the DNA chain. In chromatin, persistence length is modulated by histone packing and posttranslational modification. In vitro, DNA (cytosine methylation) and/or histone modification (acetylation) have been shown to influence chain flexibility (Brower-Toland *et al.*, 2005; Ngo *et al.*, 2016; Teng and Hwang, 2018). The relationship of epigenetic modifications of histones to the DNA mechanical code is further explored and generalized in Basu *et al.* (2021). These studies establish precedence for histone modification influence on DNA flexibility and provide a mechanical perspective on the role of epigenetic modification of the genome. Histone H2A S121 modification through Bub1 kinase is therefore a potential mechanism for altering chromatin stiffness. Increasing loop stiffness decreased the pulling force overall on centromere masses. This reduction of force in the simulation was observed in both the decreased force exerted on the centromere beads (Figure 6C) and the stretching of the springs (increased tension) connecting the centromere masses to the remainder of the pericentric chromatin (Figure 6E).

The model further allowed us to query whether alteration of pericentromere loop size and number could account for the behavior of the inner kinetochore. Increasing loop size reduced only the axial component of the force on centromere masses (Figure 7, B and D) and therefore would not cause a reduction in the radial displacement of inner kinetochore complexes observed in vivo. Additionally, increasing polymer stiffness recapitulated the paradoxical observations of reduced motion of a 10-kb lacO/LacI-GFP array located within the pericentric region and the radial expansion of the pericentric cohesin distribution in metaphase cells treated with low-dose benomyl observed in Haase *et al.* (2012). While increasing the subloop size monotonically increased the motion of a simulated array (Figure 8A) and the radial displacement of cohesin (Lawrimore *et al.*, 2016), increasing the stiffness of the simulated chromatin could either increase or decrease the motion of the simulated 10-kb array (Figure 8B) while increasing the radial displacement of cohesin (Figure 8C). Owing to the nonmonotonic relationship between simulated chromatin stiffness and the simulated array's motion (He *et al.*, 2020), it is possible to decrease the motion of the array while increasing the radial displacement of cohesin, that is, to go from a stiffness of 200 nm to 500 nm. Given the importance of posttranslational modification of the tails of histone proteins, in particular the phosphorylation of histone H2A at S121 in budding yeast via the Bub1 kinase (Kawashima *et al.*, 2010; Yamagishi *et al.*, 2010), it is possible that the effective stiffness of pericentric chromatin can be biochemically tuned by posttranslational modifications of histones. This alteration of chromatin would then result in the tuning of tension at the kinetochore, ultimately acting as a mechanism to halt mitotic progression.

In vivo modulation of chromatin stiffness prevents centromere mislocalization upon kinetochore microtubule detachment

Upon loss of attachment or reduction in tension, the pericentric chromatin is modified, reducing the probability that unattached sister chromatids will mislocalize and lead to aneuploidy. In vivo studies have shown that phosphorylation of histone H2A at S121 by Bub1 kinase is responsible for a change in the distribution of the inner kinetochore components, COMA (Haase *et al.*, 2012), and is a key regulator of chromosome segregation (Kawashima *et al.*, 2010; Yamagishi *et al.*, 2010; Nerusheva *et al.*, 2014). In addition, the C-terminus kinase domain of Bub1 and the centromere protein Sgo1 are necessary for budding yeast cells to survive spindle disassembly by the microtubule-depolymerizing drug

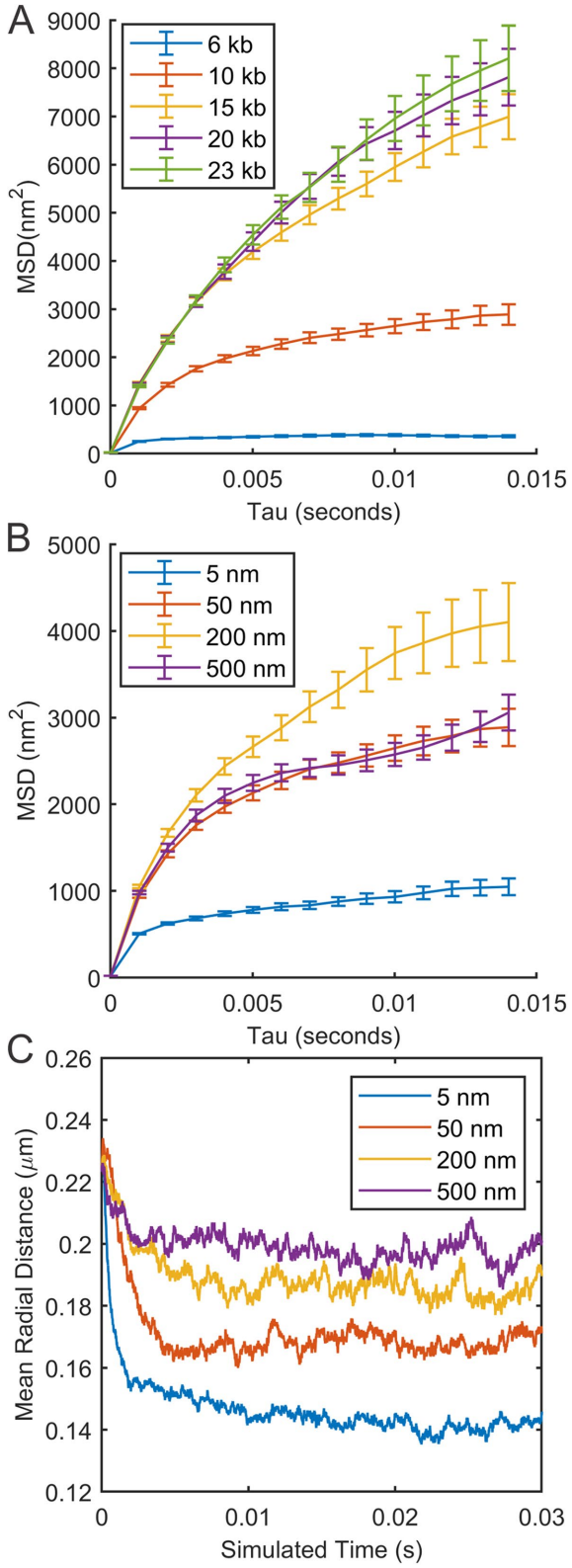

FIGURE 8: Increasing polymer stiffness has a nonmonotonic relationship with subloop motion in ChromoShake simulations. Line plots of mean squared displacement vs. tau for simulations with various loop sizes (A) and stiffnesses (B). Mean squared displacements were not calculated for the first 0.01 s to allow the simulation to reach equilibrium. (C) Line plots of the mean radial displacements of cohesin complexes over time for simulations with various polymer stiffnesses.

nocodazole (Fernius and Hardwick, 2007). Thus, modification of the pericentromeric chromatin provides a mechanism to retain features of the bottlebrush independent of the spindle apparatus. Sister kinetochores remain bioriented due to the increased stiffness of the bottlebrush, even in the absence of kinetochore microtubules. Upon microtubule regrowth, cells are able to segregate sister chromatids with sufficient fidelity to survive this perturbation. Likewise, increasing chromatin stiffness can effectively dampen the radial force and motion (Haase *et al.*, 2012) of the chromatin to prevent centromere mislocalization upon loss of kinetochore microtubule attachment. Thus, tuning the stiffness of chromatin at the pericentric region can mitigate the sister chromatid detachment from kinetochore microtubules until the opportunity to reattach arises. Chromatin-dependent tension demonstrates the critical importance of chromatin organization in the pericentric region and provides a novel perspective on tension generation and modulation at the centromere.

Chromatin-dependent tension model

The pericentric region has been considered a spring with one-dimensional tension. However, the highly looped bottlebrush model of the pericentric region simulated in this study (Figure 6A) demonstrates that a significant amount of force is exerted by the pericentromere as a consequence of the density and molecular crowding of the chromatin subloops. The tendency for loops to explore additional degrees of freedom results in a significant radial pulling force on the centromeres. Current models of sister chromatid biorientation invoke pulling forces from the kinetochore and spindle microtubules balanced by cohesive forces between sister chromatids. The polymer simulations herein offer an important addition to the current model. The highly looped nature of the pericentric bottlebrush posits that pericentric chromatin between sister kinetochores generates an entropic force. This entropic force can feed back to the kinetochore via radial contraction of the inner kinetochore components.

In the model, the sites of kinetochore microtubule attachment are pinned in place via centromere masses (i.e., the 117-base-pair site-specific centromere) with a large drag force (Lawrimore *et al.*, 2016). The simulated chromatin is initialized at its equilibrium length in metaphase. Reptation of the pericentric chromatin alone is sufficient to generate 5–10 pN at centromere masses (Figure 6), a force range consistent with previously reported forces at centromeres/kinetochore in budding yeast (Akiyoshi *et al.*, 2010; Chacon *et al.*, 2014). In simulation, the tension comes not from propagation of tension via pulling force through the chromatin that is resisted by cohesin complexes but from the entropic spring-like properties of chromatin. The extended and crowded chromatin organization in our simulations both pulls inward and expands outward due to the entropic spring force and the molecular crowding of subloops. Thus, the extended and crowded organization of pericentric chromatin can generate sufficient tension to satisfy the spindle assembly checkpoint. These forces are dependent on the packing of DNA loops and the stiffness of the chromatin chain.

MATERIALS AND METHODS

Budding yeast strain growth and benomyl treatment

Budding yeast strain KBY6397 was constructed from parent strain YEF473A (Bi and Pringle, 1996). A transforming PCR product was generated with homology to the C-terminus of Spc42 using the primers CTGAAAATAATATGTCAGAAACATTCGCAACTCCCACTCCCAATAATCGAcggatccccgggttaatta and CGTTTACGCCATTCCATTGGAACCGCAGATTGCTAGTACTATATCGTCAAgaattcgagctcgtttaaac with pFA6a-mCherry:NAT as a template to generate strain

JLY1075.1. A transforming PCR product was generated with homology to the C-Terminus of Ame1 using the primers CGGACTTCTGAAAAAGATAAATAAAATTAATGAAAATCTTTCTAACGAATTACAACCAAGTCTAcggatccccgggttaattaa and GTGCATATCTATGAAGTATGTCTACCACATAAAAATGACCTTATAACACAACTTCCTTAGTATGGgaattcgagctcgtttaaac with pFA6a-GFP:KAN as a template to generate KBY6397. The strain was grown at 24°C in yeast extract, peptone, and dextrose (YPD). For benomyl treatment, a volume of 10 mg/ml stock of benomyl in dimethyl sulfoxide was added directly to a liquid YPD culture of log-phase budding yeast to a final concentration of either 68 or 313 μM. Cells were incubated at 24°C for 45 min before imaging. Budding yeast strain KBY8022 (Figure 1B) was described in Yeh *et al.* (2008).

Budding yeast imaging

Immediately prior to imaging, yeast nitrogen base, casamino acids, uracil, tryptophan, and adenine (YPD) cultures were washed with YC complete + 2% filter sterile glucose and resuspended with YC complete + 2% filter sterile glucose. Yeast treated with benomyl were washed and resuspended with the YC complete + 2% filter sterile glucose with the same concentration of benomyl contained in the growth culture. Yeast were placed directly on glass coverslips and on glass slides. Coverslips were sealed with VALAP (equal parts Vaseline, lanolin, and paraffin). Imaging was performed at room temperature (25°C) using an Eclipse Ti wide-field inverted microscope (Nikon) with a 100 × Apo TIRF 1.49 NA objective (Nikon) and Clara charge-coupled device camera (Andor) using Nikon NIS Elements imaging software (Nikon). Images were acquired using the Scan Large Image program. Forty-nine z-stacks of seven z-steps with step size 300 nm were taken. At each interval a seven-step z-stack of 200-nm step size was acquired in the GFP (600 ms exposure), RFP (600 ms exposure), and Trans (25 ms exposure) channels. GFP, RFP, and Trans images were acquired before shifting Z position. All images were acquired from cells in the metaphase stage of the cell cycle, defined by the presence of a 1.2–1.7 μm spindle.

Image processing and analysis

Fluorescent image deconvolution was performed using Huygens Essential (Scientific Volume Imaging, Hilversum, The Netherlands).

Individual multipage TIF files were aggregated and processed for CellStar bud segmentation (Versari *et al.*, 2017). The custom MATLAB function tileProcess.m aggregates the multipage TIF files into multipage TIF files for each channel, GFP, RFP, and Trans. The Trans channel contains only the middle focal plane image. The tileProcess.m produces a median intensity projection image for the background subtraction image that is passed into CellStar. A custom MATLAB program, batchSelection.m, runs CellStar to segment the buds from the Trans images, applies the segmentation masks to the GFP and RFP channels, filters the GFP/RFP segments to include only images with two foci that meet a specified signal-to-noise ratio. The code utilizes the function advPointSourceDetection.m (Ciccconet *et al.*, 2017), which was developed based on code developed by Francois Aguet (Aguet *et al.*, 2013). The custom MATLAB function, spotHeightStructure.m, was called on the MAT-files produced by batchSelection.m to filter cells by kinetochore position relative to spindle pole bodies, foci intensity distribution, and to remove images with fuzzy signals. The width of the foci was measured by cropping a 7 × 15 pixel (width by height) region, 451.5 × 967.5 nm, from segmented images that were rotated to align the spindle pole bodies to the horizontal axis. The cropped region was sum projected across the width to produce an array of 15 integrated intensity values. These values were fitted to a Gaussian using MATLAB's nonlinear least squares method of MATLAB's fit function. The full-width-half-max (FWHM), σ^* 2.355, of the fitted Gaussian curve was calculated for all foci. The distributions of Ame1-GFP foci heights and Spc42-mCherry foci heights were filtered by iteratively applying MATLAB's isoutlier function until no outliers were detected. The isoutlier function labels observations that are more than three scaled median absolute deviations from the median. The MATLAB code to run the above analysis can be found at https://github.com/jlaw8504/CellStarSelect.

The intensity measurements of the Ame1-GFP foci were performed using the custom MATLAB program intensity_quant.m. This program parses imaging data stored in MAT files from the CellStarSelect program. Images of Ame1-GFP foci segmented from background noise and the intensity values were background subtracted using MATLAB's multithresh.m function based on Otsu's thresholding (Otsu, 1979). The number and intensity values of Ame1-GFP foci were used to calculate the integrated intensity of foci, the mean intensity of foci, the mean intensity per cubic micron, and the maximum intensity value per voxel per foci. The intensity_quant.m program is found at https://github.com/BloomLabYeast/radial_tension/tree/main/Figure3_ame1_compression.

KineticButShakeless synthetic image generation and analysis

The custom MATLAB application KineticButShakeless (https://github.com/BloomLabYeast/KineticButShakeless) was used to create simulated images of kinetochore proteins by interfacing with Microscope Simulator 2 (Quammen *et al.*, 2008). The entire kinetochore complex is simulated as a 70-nm-long vector. The number of vectors and their orientations in three-dimensional space can be specified by the user (Lawrimore *et al.*, 2019). The synthetic images were analyzed using a modified version of CellStarSelect pipeline that did not require bud segmentation (https://github.com/jlaw8504/CellStarSelect/tree/Zach).

ChromoShake polymer simulations

ChromoShake centromere models with various subloop sizes were generated using chromoShake_make_spindle.cpp (Lawrimore *et al.*, 2016). Note that the MSI installer of ChromoShake does not contain the loop_expansion flag tag. Download source code (http://bloomlab.web.unc.edu/wp-content/uploads/sites/11326/2016/01/Source_code.zip) and compile for version of chromoShake_make_spindle.cpp with ability to alter radial subloop size. To generate simulations with various polymer stiffnesses, the default centromere simulation was produced using chromoShake_make_spindle.cpp and all hinge forces were replaced in the resulting configuration file with hinge forces corresponding to persistence lengths of 500 nm, hinge force value of 4.0715×10^{-11}, and 200 nm, hinge force value of 1.6286×10^{-11}. The hinge forces were deleted from the configuration file to generate a simulation with a persistence length of 5 nm. In the simulation, beads are separated by 10 nm. The distance over which two monomer units within a polymer move independently is two times the persistence length. Thus, no hinge forces correspond to a persistence length of 5 nm.

ChromoShake tension analysis

Tension on centromere masses was measured by calculating the change in distance between sister centromere masses over time and calculating the force required to move the centromere beads at the measured velocity. Centromere masses in the simulation have 10^5 higher viscosity applied to them than other beads, effectively pinning them in space. However, the centromere masses were observed to

move over time. This drag-based analysis was performed using the custom MATLAB pipeline end_to_end (all code on GitHub at https://github.com/BloomLabYeast/radial_tension/tree/main/end_to_end). An alternative method to measure tension in ChromoShake simulations is to monitor the extension of the Hookean springs joining the masses. This analysis was performed using the custom Python code TensionSim (https://github.com/jlaw8504/chromoSnake/tree/tension). Demonstrations of how to use TensionSim are available in the Jupyter Notebooks found here: https://github.com/BloomLabYeast/radial_tension/blob/main/tensionSim_persistence_lengths.html and https://github.com/BloomLabYeast/radial_tension/blob/main/tensionSim_persistence_lengths.ipynb

ChromoShake MSD and cohesin radial displacement

The mean squared displacement of a simulated 10-kb lacO/LacI-GFP array were calculated using the published bead position files (Lawrimore *et al.*, 2016) at (http://bloomlab.web.unc.edu/wp-content/uploads/sites/11326/2016/01/MSD_scripts.zip) and the coordinate_summary.cpp program. The coordinate summary CSV files were imported into MATLAB using the custom MATLAB function parse_coord_summary.m. The mean squared displacement curves were calculated using the custom MATLAB program equib_msd_summary.m, where the first 1000 printed time points (0.01 s, 2 ns per calculation, and 5000 calculations per printed time step) were excluded to allow for the simulation to equilibrate. The source code can be found here: https://github.com/BloomLabYeast/radial_tension/tree/main/msd_analysis_size. The radial displacement of cohesin was calculated using the program cohesin_summary.cpp (Lawrimore *et al.*, 2016) with the cohesin_src.txt file (https://github.com/BloomLabYeast/radial_tension/blob/main/cohesin_src.txt) that specifies the cohesin masses in the default centromere simulation produced by chromoShake_make_spindle.cpp.

Code availability

All code will be published to a GitHub repository upon publication.

ACKNOWLEDGMENTS

We thank the members of the Bloom laboratory for suggestions and critical reading of the manuscript. This work was supported by NIH R37GM32238 to K.B.

REFERENCES

Aguet F, Antonescu CN, Mettlen M, Schmid SL, Danuser G. (2013) Advances in analysis of low signal-to-noise images link dynamin and AP2 to the functions of an endocytic checkpoint. Dev Cell 26, 279–291.

Akiyoshi B, Sarangapani KK, Powers AF, Nelson CR, Reichow SL, Arellano-Santoyo H, Gonen T, Ranish JA, Asbury CL, Biggins S (2010). Tension directly stabilizes reconstituted kinetochore-microtubule attachments. Nature 468, 576–579.

Basu A, Bobrovnikov DG, Ha T (2021). DNA mechanics and its biological impact. J Mol Biol 433, 166861.

Bi E, Pringle JR (1996). ZDS1 and ZDS2, genes whose products may regulate Cdc42p in Saccharomyces cerevisiae. Mol Cell Biol 16, 5264–5275.

Biggins S (2013). The composition, functions, and regulation of the budding yeast kinetochore. Genetics 194, 817–846.

Brower-Toland B, Wacker DA, Fulbright RM, Lis JT, Kraus WL, Wang MD (2005). Specific contributions of histone tails and their acetylation to the mechanical stability of nucleosomes. J Mol Biol 346, 135–146.

Chacon JM, Mukherjee S, Schuster BM, Clarke DJ, Gardner MK (2014). Pericentromere tension is self-regulated by spindle structure in metaphase. J Cell Biol 205, 313–324.

Cicconet M, Hochbaum DR, Richmond D, Sabatini BL (2017). Bots for software-assisted analysis of image-based transcriptomics. ICCVW, 134–142. doi:10.1109/ICCVW.2017.24.

Dhatchinamoorthy K, Shivaraju M, Lange JJ, Rubinstein B, Unruh JR, Slaughter BD, Gerton JL (2017). Structural plasticity of the living kinetochore. J Cell Biol 216, 3551–3570.

Fernius J, Hardwick KG (2007). Bub1 kinase targets Sgo1 to ensure efficient chromosome biorientation in budding yeast mitosis. PLoS Genet 3, e213.

Haase J, Mishra PK, Stephens A, Haggerty R, Quammen C, Taylor RM 2nd, Yeh E, Basrai MA, Bloom K (2013). A 3D map of the yeast kinetochore reveals the presence of core and accessory centromere-specific histone. Curr Biol 23, 1939–1944.

Haase J, Stephens A, Verdaasdonk J, Yeh E, Bloom K (2012). Bub1 kinase and Sgo1 modulate pericentric chromatin in response to altered microtubule dynamics. Curr Biol 22, 471–481.

Hagerman PJ (1988). Flexibility of DNA. Annu Rev Biophys Biophys Chem 17, 265–286.

He Y, Lawrimore J, Cook D, Van Gorder EE, De Larimat SC, Adalsteinsson D, Forest GM, Bloom K (2020). Statistical mechanics of chromosomes:in vivo and in silico approaches reveal high-level organization and structure arise exclusively through mechanical feedback between loop extruders and chromatin substrate properties. Nucleic Acids Res 48, 11284–11303.

Henderson SA, Koch CA (1970). Co-orientation stability by physical tension: a demonstration with experimentally interlocked bivalents. Chromosoma 29, 207–216.

Kawashima SA, Yamagishi Y, Honda T, Ishiguro K, Watanabe Y (2010). Phosphorylation of H2A by Bub1 prevents chromosomal instability through localizing shugoshin. Science 327, 172–177.

Lawrimore J, Aicher JK, Hahn P, Fulp A, Kompa B, Vicci L, Falvo M, Taylor RM 2nd, Bloom K (2016). ChromoShake: a chromosome dynamics simulator reveals that chromatin loops stiffen centromeric chromatin. Mol Biol Cell 27, 153–166.

Lawrimore J, Doshi A, Friedman B, Yeh E, Bloom K (2018). Geometric partitioning of cohesin and condensin is a consequence of chromatin loops. Mol Biol Cell 29, 2737–2750.

Lawrimore J, Doshi A, Walker B, Bloom K (2019). AI-assisted forward modeling of biological structures. Front Cell Dev Biol 7, 279.

Lawrimore J, Vasquez PA, Falvo MR, Taylor RM 2nd, Vicci L, Yeh E, Forest MG, Bloom K (2015). DNA loops generate intracentromere tension in mitosis. J Cell Biol 210, 553–564.

Li X, Nicklas RB (1995). Mitotic forces control a cell-cycle checkpoint. Nature 373, 630–632.

Nerusheva OO, Galander S, Fernius J, Kelly D, Marston AL (2014). Tension-dependent removal of pericentromeric shugoshin is an indicator of sister chromosome biorientation. Genes Dev 28, 1291–1309.

Ngo TTM, Yoo J, Dai Q, Zhang Q, He C, Aksimentiev A, Ha T (2016). Effects of cytosine modifications on DNA flexibility and nucleosome mechanical stability. Nat Commun 7, 10813.

Nicklas RB, Koch CA (1969). Chromosome micromanipulation. 3. Spindle fiber tension and the reorientation of mal-oriented chromosomes. J Cell Biol 43, 40–50.

O'Toole ET, Winey M, McIntosh JR (1999). High-voltage electron tomography of spindle pole bodies and early mitotic spindles in the yeast Saccharomyces cerevisiae. Mol Biol Cell 10, 2017–2031.

Otsu N (1979). A threshold selection method from gray-level histograms. IEEE Trans Sys Man Cyber 9, 62–66.

Paldi F, Alver B, Robertson D, Schalbetter SA, Kerr A, Kelly DA, Baxter J, Neale MJ, Marston AL (2020). Convergent genes shape budding yeast pericentromeres. Nature 582, 119–123.

Panyukov S, Zhulina EB, Sheiko SS, Randall GC, Brock J, Rubinstein M (2009a). Tension amplification in molecular brushes in solutions and on substrates. J Phys Chem B 113, 3750–3768.

Panyukov SV, Sheiko SS, Rubinstein M (2009b). Amplification of tension in branched macromolecules. Phys Rev Lett 102, 148301.

Pearson CG, Maddox PS, Zarzar TR, Salmon ED, Bloom K (2003). Yeast kinetochores do not stabilize Stu2p-dependent spindle microtubule dynamics. Mol Biol Cell 14, 4181–4195.

Quammen CW, Richardson AC, Haase J, Harrison BD, Taylor RM, Bloom KS (2008). FluoroSim: a visual problem-solving environment for fluorescence microscopy. Eurographics Workshop Vis Comput Biomed 2008, 151–158.

Rubinstein M, Colby RH (2003). Polymer Physics, Oxford, UK: Oxford University Press.

Smith SB, Cui Y, Bustamante C (1996). Overstretching B-DNA: the elastic response of individual double-stranded and single-stranded DNA molecules. Science 271, 795–799.

Stephens AD, Haggerty RA, Vasquez PA, Vicci L, Snider CE, Shi F, Quammen C, Mullins C, Haase J, Taylor RM 2nd, *et al*. (2013a). Pericentric chromatin loops function as a nonlinear spring in mitotic force balance. J Cell Biol 200, 757–772.

Stephens AD, Quammen CW, Chang B, Haase J, Taylor RM 2nd, Bloom K (2013b). The spatial segregation of pericentric cohesin and condensin in the mitotic spindle. Mol Biol Cell 24, 3909–3919.

Suzuki A, Badger BL, Haase J, Ohashi T, Erickson HP, Salmon ED, Bloom K (2016). How the kinetochore couples microtubule force and centromere stretch to move chromosomes. Nat Cell Biol 18, 382–392.

Teng X, Hwang W (2018). Effect of methylation on local mechanics and hydration structure of DNA. Biophys J 114, 1791–1803.

Versari C, Stoma S, Batmanov K, Llamosi A, Mroz F, Kaczmarek A, Deyell M, Lhoussaine C, Hersen P, Batt G (2017). Long-term tracking of budding yeast cells in brightfield microscopy: CellStar and the Evaluation Platform. J R Soc Interface 14, 20160705.

Winey M, Mamay CL, O'Toole ET, Mastronarde DN, Giddings TH Jr, McDonald KL, McIntosh JR (1995) Three-dimensional ultrastructural analysis of the Saccharomyces cerevisiae mitotic spindle. J Cell Biol 129, 1601–1615.

Yamagishi Y, Honda T, Tanno Y, Watanabe Y (2010). Two histone marks establish the inner centromere and chromosome bi-orientation. Science 330, 239–243.

Yeh E, Haase J, Paliulis LV, Joglekar A, Bond L, Bouck D, Salmon ED, Bloom KS (2008). Pericentric chromatin is organized into an intramolecular loop in mitosis. Curr Biol 18, 81–90.

Yoo TY, Choi JM, Conway W, Yu CH, Pappu RV, Needleman DJ (2018). Measuring NDC80 binding reveals the molecular basis of tension-dependent kinetochore-microtubule attachments. eLife 7, e36392.